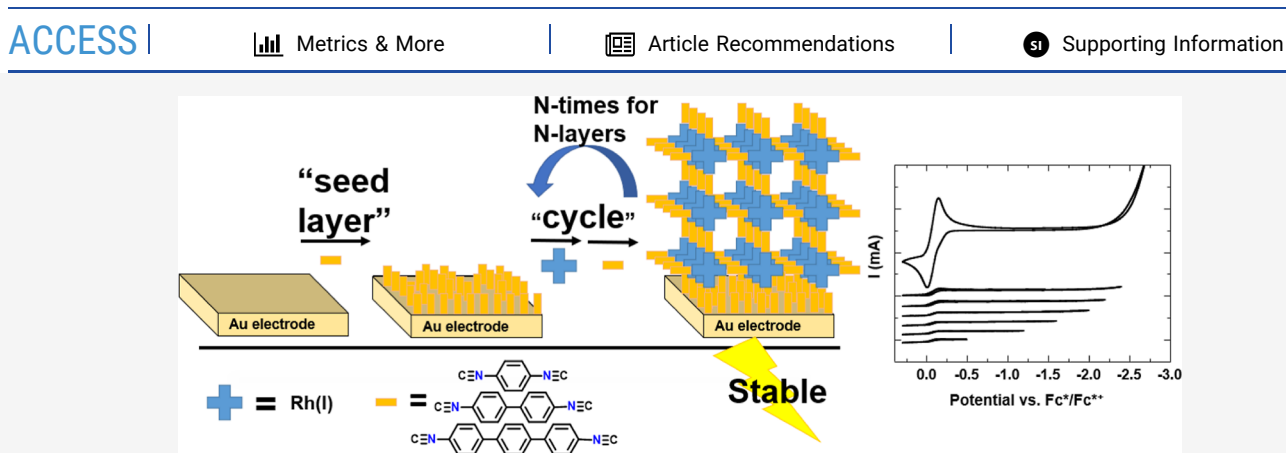


pubs.acs.org/JPCC Article

Layer-by-Layer Deposition of Rh(I) Diisocyanide Coordination Polymers on Au(111) and Their Chemical and Electrochemical Stability

Gwendolynne L. Lee, Thomas Chan, Joseph M. Palasz, and Clifford P. Kubiak*





ABSTRACT: The synthesis of electrode-attached Rh(I) diisocyanide coordination polymers that incorporate a series of arylene diisocyanide linkers and which are grown from gold surfaces by a bottom-up, layer-by-layer procedure that allows for a high level of control for the film thickness is reported. A seed layer of the arylene diisocyanide ligand is used to template directional growth of the coordination polymer made using the well-studied square-planar rhodium tetrakis(isocyanide) as the metal node. Materials ranging from 1 to 30 layers were prepared via layer-by-layer solution-phase deposition. Characterization of the polymer films using scanning electron microscopy and ellipsometry shows layer-by-layer control in these films with linear thickness growth per layer. Phase-modulated infrared reflection absorption spectroscopy (PM-IRRAS), diffuse reflectance UV-vis, and X-ray photoelectron spectroscopy (XPS) were used to confirm the structures of the films. Although prior reports of related coordination polymers and films based on diisocyanides showed considerable air-instability, the films reported here demonstrate significantly improved chemical stability and electrochemical stability at a moderately high applied bias. Electrochemical characterization and ex situ XPS demonstrate that these diisocyanide films are stable to stripping at potentials up to -2.2 V versus decamethylferrocene in acetonitrile, supporting their relevance for electrochemical applications.

INTRODUCTION

The heterogenization of molecular electrocatalysts is appealing for improving recyclability, reducing the required catalyst loading, and arresting catalyst deactivation pathways. Molecular catalysts offer high selectivity and are generally well understood mechanistically. Prior attempts to heterogenize molecular catalysts include covalent or chemisorbed attachment in self-assembled monolayers, Polymers, and attachment in metal—organic frameworks (MOFs). Heterogenizing molecular catalysts can offer improved catalytic performance and enable catalysis in environments previously restricted by solubility. The porosity of MOFs is particularly attractive for electrochemical applications since the three-dimensional MOF structure can be used to create a highly ordered network of catalyst sites that are immobilized on the activating electrode surface. Such materials hold the potential to enable the large-scale electrochemical conversion

of various interesting substrates such as CO₂, H₂O, H₂, O₂, and ethylene.

Porous hybrid materials, ranging from amorphous coordination polymers¹³ and ordered MOFs,¹⁴ are often constructed in manners that intrinsically lead to low electrical conductivity, which presents a major obstacle for their use in electrochemical applications.¹⁵ While recent work has demonstrated that MOFs containing cobalt porphyrin linkers achieve electronic conductivity by charge hopping from linker to linker,¹⁶ MOFs that exhibit through-bond conductivity, particularly via metal—

Received: July 18, 2022
Revised: September 2, 2022
Published: September 15, 2022





metal orbital overlap, are less common and unexplored for electrocatalysis 17 or conductive materials. 15

Rhodium diisocyanide coordination polymers, first reported by Feinstein-Jaffe, are expected to have anisotropic electrical conductivity. The proposed structure of these materials is depicted in Figure 1. The chloride counterions are omitted for

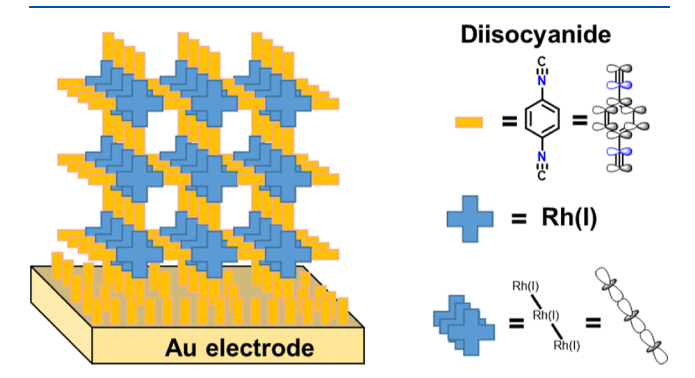
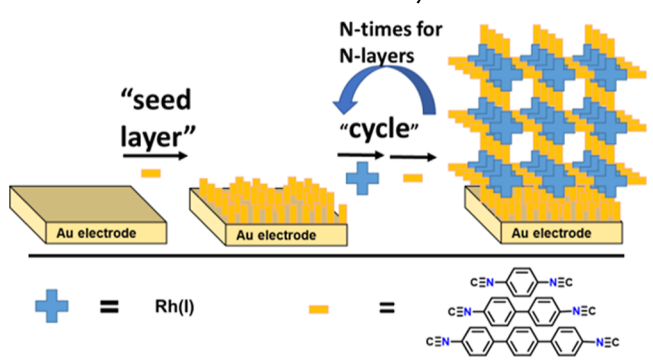


Figure 1. Expected structure of Rh(I) diisocyanide coordination polymers. The inset portrays the π -conjugation expected for the PDI linker and the d_z^2 orbital overlap expected for Rh(I) atoms in the stacked coordination polymer structure. The chloride counterions were omitted for clarity.

Scheme 1. Layer-by-Layer Coordination Polymer Growth Starting with a Seed Layer of Diisocyanide; the Chloride Counterions Were Omitted for Clarity



clarity in Figure 1 and Scheme 1. The Rh(I) centers of Rh(I)tetrakis-isocyanides are known to form extended stacks through Rh-Rh bonding, 18 and this behavior has been applied to form nanowires with conductivity on the order of 10^{-3} S/ cm. 19 While the axis along Rh-Rh stacking can display high conductivity if well ordered, the other axes are expected to have semiconductor or insulating behavior consistent with a network of the aryl ligand π^* -orbitals. The oligomerization through Rh-Rh stacking is indicated in previously studied diisocyanide coordination polymer analogues by the powder Xray diffraction (PXRD) pattern and reflectance UV-vis, but the reported bulk conductivity of these materials is in the lowsemiconductor range (10^{-4} S/cm) , and a recent report puts it closer to the insulative range (10^{-8} S/cm) . It is likely that defects and grain boundaries in the polycrystalline materials significantly attenuate the high conductivity that could arise in an organized structure, as suggested by the modest evidence of crystallinity by PXRD.²⁰ The presence of isocyanate impurities due to isocyanide oxidation upon air and moisture exposure

may also contribute to the disordered structure and low conductivity of these bulk materials.²⁰

For the development of porous structures that may be relevant for electrochemical applications such as sensing and the heterogenization of electrocatalysts, a highly ordered network is needed such that the material can be capable of electronic communication with the electrode. With these goals in mind, we targeted the epitaxial growth of Rh(I) diisocyanide coordination polymers from an electrode surface. Herein, we report the development of Rh(I) diisocyanide coordination polymers grown layer-by-layer on Au(111) surfaces. The films are structurally characterized, and their electrochemical stability is evaluated.

■ EXPERIMENTAL SECTION

General Considerations. Solvents were dried in a solvent system equipped with drying columns and inert gas for exclusion of oxygen prior to syntheses. Solvents in electrochemical testing were degassed by sparging with argon.

Materials and Chemical Reagents. 1,4-Phenylenediisocyanide (PDI) was purchased from Sigma-Aldrich (97%), benzidine was purchased from Sigma-Aldrich (≥98%), 4,4"diamino-p-terphenyl was purchased from Lancaster (95%), formic acid was purchased from Fischer Chemical (88%), phosphorus oxychloride was purchased from Spectrum Chemical (≥98%), rhodium(I) dicarbonyl chloride dimer was purchased from Sigma Aldrich (97%), tert-butyl isocyanide (tBuNC) was purchased from Sigma-Aldrich (98%), concentrated sulfuric acid was purchased from Fischer Chemicals, and hydrogen peroxide was purchased from Fischer Chemicals (30%); all the preceding chemicals were used as received. Triethylamine was purchased from Acros Chemical (99%) and dried over 4 Å molecular sieves. Tetrabutylammonium hexafluorophosphate (TBAPF₆) was purchased from TCI (≥98%), recrystallized from hot ethanol, and dried in a vacuum oven.

4,4'-Diisocyanide-biphenyl. 4,4'-Diisocyanide-biphenyl (BPDI) was synthesized by modification of a literature method. Benzidine (241.05 mg, 1.31 mmol) was dissolved in 2 mL of 88% formic acid and stirred for 18 h. The reaction was then quenched by addition of 20 mL of saturated sodium carbonate solution. The **4,4'-diformamide-biphenyl** product formed as a pale precipitate was isolated by filtration, washed with ethanol, and dried in a vacuum oven at 100 °C. For the subsequent dehydration of the diformamide to the BPDI, the reaction was performed as previously described but allowed to proceed at room temperature for 20 h (60% yield, characterization matched that previously described for this compound). ²²

4,4"-Diisocyanide-*p*-terphenyl. 4,4"-Diisocyanide-*p*-terphenyl (TPDI) was synthesized from 205.10 mg of 4,4"-diamino-*p*-terphenyl (0.788 mmol) in an analogous fashion as the synthesis of BPDI. (32% yield, characterization matched that previously described for this compound).²³

Rhodium(I) Tetrakis(t-butyl Isocyanide) Chloride. In a glovebox, 250.10 mg (3.01 mmol) of tBuNC was dissolved in 2 mL of dry dichloromethane and added dropwise to a stirred solution of 107.02 mg [Rh(CO)₂Cl]₂ (0.275 mmol) in 5 mL of dry dichloromethane at room temperature. After 6 h, the product was dried in vacuo to remove the solvent and excess tBuNC until the mass stabilized to near quantitative conversion with respect to rhodium. [94% yield, (241.8 mg, 0.4808 mmol)]. ¹H NMR (500 MHz, CD₂Cl₂): δ 1.50 (m)

ppm. 13 C NMR (125 MHz, CD₂Cl₂): δ 136.62, 58.62, 30.59 ppm. IR (CH₂Cl₂ solution) matched that previously described for this compound. 24

Gold Substrate Preparation. Glass microscope slides were positioned in a Denton 18 sputter coater. At a 200 W power and 2.5 mTorr pressure of argon, a Ti adhesion layer was first applied for 15 s, and then the Au layer was sputtered for 120 s. The nominal gold thickness was 200 nm. The sputtered slides were cut to approximately (1 × 2.5) cm² pieces and cleaned in a hot piranha solution (1:3 30% $\rm H_2O_2/H_2SO_4$) for 30 min. Following the piranha etch, slides were rinsed copiously with deionized water and stored in 18 MΩ water until use for film preparation or as control samples for electrochemistry, phase-modulated infrared reflection absorption spectroscopy (PM-IRRAS), and X-ray photoelectron spectroscopy (XPS) measurements. Prior to use, samples were rinsed with methanol and then dichloromethane.

Solution-Phase Atomic Layer Deposition of Multilayers. The deposition procedures are graphically depicted in Scheme 1. Method A, dropcast preparation at ambient lab conditions: This procedure was performed with all diisocyanides (PDI, BPDI, and TPDI). 5 mM solutions of PDI, BPDI, and TPDI were prepared in dichloromethane and filtered with 0.2 µM PTFE syringe filters. Dense seed layers of each diisocyanide were prepared on gold slides by soaking 2 cm × 1 cm pieces of slides in the 5 mM solutions for 24 h. After the seed layer, slides were washed with dichloromethane, and then dichloromethane solutions of the Rh(tBuNC)₄Cl (2 mM) and diisocyanide linker (5 mM) were alternately applied by a pipette to the slide, with a waiting time of 1 min followed by a rinse with dichloromethane. A cycle is defined as one iteration of Rh(tBuNC)₄Cl and diisocyanide linker application after the initial seed layer. Samples were immediately stored in vials flushed with nitrogen and sealed until measurement.

Method B, air-free preparation was performed for films of Rh(I) BPDI in a glovebox: The seed layer of the diisocyanides was prepared as described above for Method A. A 5 mM solution of BPDI in dichloromethane was prepared and filtered with 0.2 μ M PTFE syringe filters. A dense seed layer of the diisocyanide on a gold slide was prepared by soaking the slide in the filtered solution for 24 h. Multilayers were then prepared by alternately dipping the slide into a 1 mM [Rh(CO)₂CI]₂ solution and the solution of diisocyanide. The slides were rinsed with dichloromethane between each diisocyanide and [Rh(CO)₂Cl]₂ dip to avoid the formation of disordered aggregates due to adhered droplets of reagent solution.

Instrumentation. 1 H and 13 C NMR spectra were taken using a Bruker 300 MHz NMR or Varian 500 MHz NMR instrument. All NMR spectra were recorded at room temperature. Chemical shifts are reported in parts per million (δ). FT-IR spectra were taken on ca. 1 mg/mL solution in a Specac CaF₂ IR cell using a ThermoScientific Nicolet 6700 FT-IR spectroscope with 16 scans over the range of 400–4000 cm⁻¹ and resolution of 4 cm⁻¹. Solvent subtraction and baseline correction were performed.

PM-IRRAS was performed using a Bruker Equinox 55 with external PMA-37 accessory. Polarization modulation was achieved using a PEM-90-D ZnSe photoelastic modulator (Hinds Instruments) operating at 50 kHz and half-wave retardation coupled with a synchronous sampling demodulator (GWC Instruments). The reflected light was detected with a liquid nitrogen cooled mercury cadmium telluride detector with a BaF₂ window. Spectra were collected with 30 scans from

500 to 4000 cm⁻¹, a resolution of 4 cm⁻¹, maximum dephasing set to 2000 cm⁻¹, and a detector angle of 87.5° with respect to the surface normal. Spectra were collected in a nitrogen atmosphere using a Parker Balston purge gas generator. A linear least-squares array baseline in OriginPro software was used for baseline correction to remove artifacts from the Bessel function, and a baseline-corrected spectrum of a clean gold sample was subtracted to remove the characteristic gold background. PM-IRRAS data were collected with no more than 30 min of air exposure time for each sample post-preparation, except in instances in which PM-IRRAS measurements were performed again after exposing the sample to electrochemical testing.

Ellipsometry was performed using a Rudolph Auto EL ellipsometer with a wavelength of 632.8 nm, and three spots per sample were measured. Δ and Ψ values were recorded, and iterative fitting of Ψ values to a model of a film with refractive index n=1.5 and absorption coefficient k=0 on gold was used to find thickness. The gold refractive index and absorption coefficient were calculated from the Δ and Ψ values of a clean gold sample. Ellipsometry data were collected with no more than 2 days of air exposure time for each sample post-preparation.

Diffuse reflectance UV—vis spectra were collected using a Perkin Elmer lambda 1050 UV—vis—NIR spectrophotometer using the Universal Reflectance Accessory. Spectra were collected with 10 nm resolution from 200 to 800 nm with a data interval of 10 nm and a scan speed of 5 nm/s. The Kubelka—Munk equation was used to convert transmission spectra to absorbance spectra by the equation $F(R) = (1 - R)^2/2R$, and a spectrum of a clean gold substrate was subtracted from the sample spectra to obtain background-corrected data.

XPS was performed using an AXIS Supra instrument at the UC Irvine Materials Research Institute. Spectra were referenced and fit using the CasaXPS software. The survey spectra were indexed to 284.8 eV for carbon. In the high-resolution C 1s spectra, the most dominant carbon peak component was indexed to 284.8 eV. In the high-resolution N 1s spectra, the most dominant nitrogen peak component was indexed to 400.2 eV. For other high-resolution spectra, the same offset used for the C 1s XPS data was applied. XPS readings were collected on samples with no more than 1 week of air exposure time post-preparation.

Electrochemical experiments were performed using a three-electrode setup with the modified gold surfaces as the working electrode, a platinum counter electrode, and an Ag/AgCl reference electrode. The areas of the gold working electrodes were controlled to approximately 1 cm². Cyclic voltammetry was carried out in dichloromethane or acetonitrile with a 0.1 M tetra-n-butylammonium hexafluorophosphate (TBAPF₆) and a 2 mM decamethylferrocene (Fc*) internal standard. The potential was scanned at 50 mV/s to successively more cathodic potentials. Voltammetry was performed on samples with no more than 1 day of air exposure time post-preparation.

■ RESULTS AND DISCUSSION

Layer-by-Layer Control of Coordination Polymer Growth. Ellipsometry was used to evaluate the progress of the layer-by-layer deposition of the Rh(I) coordination polymers. Data for the seed diisocyanide layers on gold and the multilayers for each coordination polymer prepared with PDI, BPDI, and TPDI by method A are shown in Figure 2.

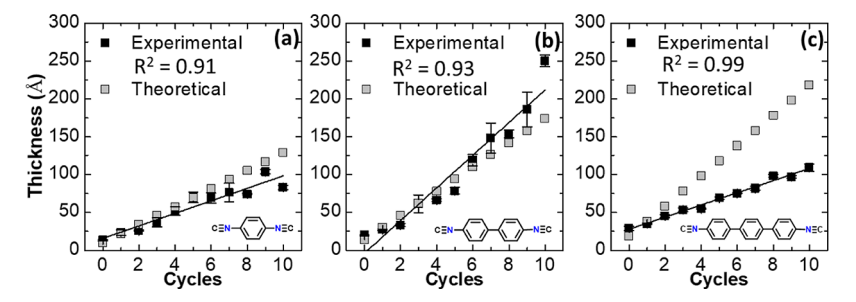


Figure 2. Ellipsometric thickness of Rh(I) PDI films (left), Rh(I) BPDI films (middle), and Rh(I) TPDI films (right). Experimental data of the average thicknesses are plotted in black squares with blue error bars denoting ± 1 standard deviation. Theoretical data are plotted in gray squares.

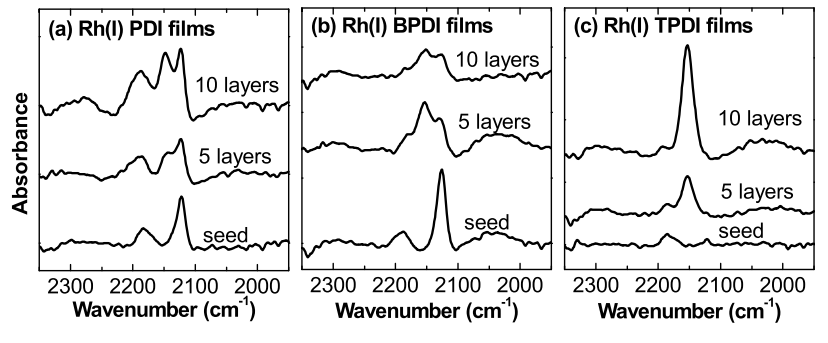


Figure 3. PM-IRRAS spectra of Rh(I) PDI (a), Rh(I) BPDI (b), and Rh(I) TPDI (c) films prepared by method A.

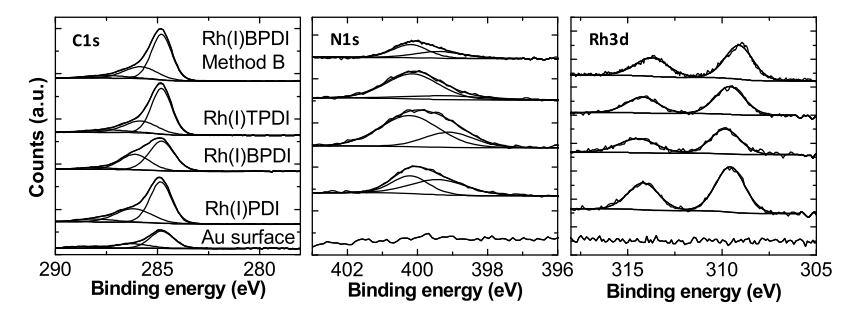


Figure 4. C 1s, N 1s, and Rh 3d high-resolution XPS (left to right) of a gold surface and Rh(I) diisocyanide films grown layer-by-layer on gold surfaces. The order of samples indicated in the C1s spectra is consistent for the N 1s and Rh 3d plots. All films measured were prepared by 10 dipping cycles after the seed diisocyanide layer. The quantification component peaks are shown, and their sum is also shown overlapping closely with the raw spectra.

Assuming perpendicular growth orientation of the coordination polymer, films with PDI linkers would be expected to show a seed layer thickness of 10.0 Å, corresponding to the *y*-intercept, and a growth of 11.9 Å angstroms per cycle of Rh(I) and PDI, corresponding to the slope of the graph. The experimental data are in good agreement with the theoretical calculations. The films with BPDI linkers would be expected to show an intercept of 14.1 Å and a slope of 16.0 Å, and while the data have some noise at higher thicknesses and therefore the intercept does not match what is expected, evidence of layer-by-layer control is clearly indicated. The data for PDI and BPDI layers show successful layer-by-layer deposition and indicate perpendicular orientation of growth of the coordination polymer.

In contrast, the films constructed with TPDI as the linker between Rh(I) surfaces show multilayer thickness growth per cycle of Rh(I) and TPDI shows layer-by-layer thickness growth that is less than expected for perpendicular growth. The overall result is consistent with a tilt angle of 26.2° relative to the gold surface based on the slope of 8.0 Å shown in Figure 2C rather than the expected slope of 18.1 Å. Similar findings of leaning

orientation have been reported with others on self-assembled monolayers (SAMs) with aromatic isocyanides of comparable length.²⁵ This behavior likely results from competition between the preferred perpendicular orientation of the Auisocyanide bond and dispersion forces favoring a flat, parallel orientation. This is not unexpected considering the relatively long 18.1 Å length of TPDI compared to the shorter phenyl (PDI) and biphenyl (BPDI) diisocyanides.

The PM-IRRAS spectra provide additional support of multilayer growth based on increasing intensities of expected diisocyanide IR vibrational stretching frequencies. Figure 3a—c shows the isocyanide region of the PM-IRRAS spectra for the multilayers based on PDI, BPDI, and TPDI, respectively, prepared by method A. The seed layer diisocyanides and the multilayer films show distinct $C \equiv N$ stretches for gold-bound, Rh(I)-bound, and free aryl isocyanide: 2185, 2165, and 2120 cm⁻¹, respectively. While peaks for the $C \equiv N$ stretch from each isocyanide bonding environment are observed in all films, the gold-bound and free isocyanide features are most prominent for the Rh(I) PDI films. The retention of the free $C \equiv N$ stretch in the layered films indicates some unreacted

seed layer being conserved in the deposition, likely remaining unbound due to the seed layer packing more densely than the coordination polymer overlayers. The weak intensity of gold-bound and free isocyanide in the seed TPDI layer and Rh(I) TPDI multilayers is consistent with a non-perpendicular orientation of the polymer, as indicated by the ellipsometry data, since the PM-IRRAS surface selection rules dictate that the degree to which the IR stretch vector is perpendicular to the surface of the sample will be proportional to the intensity of the measured absorbance. Thus, the PM-IRRAS data support that the thickness increases detected by ellipsometry are indicative of controlled growth of the intended structure. In addition to the presence of Rh(I)-bound isocyanide stretches, Rh 3d XPS also confirms the presence of isocyanide ligands coordinated to rhodium in each film (Figure 4).

Rh–Rh Oligomerization in the Multilayer Films. The presence of extensive Rh–Rh oligomerization in the films is a desired property because it is expected to result in conductive behavior along the Rh–Rh channels. Rh–Rh oligomerization is known to create absorbances in the visible range in the 600–700 nm region^{7,18} and was thus assessed in the films using reflectance UV–vis–NIR spectroscopy. The spectra of 10 and 30 multilayer samples of the Rh(I) BPDI films prepared by method A (Figure 5) show absorbances at 700 nm in addition

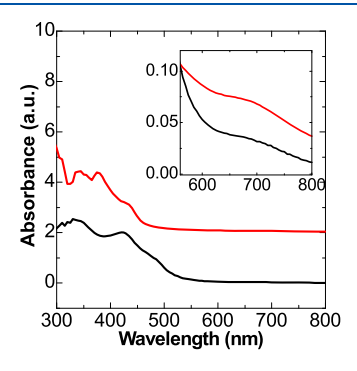


Figure 5. Diffuse-reflectance UV—vis spectra of Rh(I) BPDI films of 10 (black) and 30 (red) layers. The inset shows the weak absorbance in the region indicative of Rh—Rh bonding.

to stronger metal ligand charge transfer (MLCT bands) at lower wavelengths. The UV-vis-NIR spectra are consistent with Rh-Rh oligomerization, leading to a d_z^2 orbital overlap in the film.

Evaluation of Impurities in the Multilayer Films. Because isocyanide SAMs and coordination polymers have been previously described as showing instability to ozone in ambient air, leading to the formation of isocyanate or polyisocyanide functional groups, 20,26 PM-IRRAS and XPS data were evaluated for the formation of these impurities. In PM-IRRAS data, isocyanates and polyisocyanides are expected to show C=N stretches at 2267 and 1570-1670 cm⁻¹, respectively.²⁰ For the Rh(I) films, the multilayers prepared by method A show some polyisocyanide signal (Figure S1), but none of the films shows evidence of isocyanates (Figure 3). High-resolution C 1s XPS spectra of the Rh(I) diisocyanide films show large signals at 284.8 and 286 eV, consistent with aromatic and isocyanide carbon, respectively (Figure 4).²⁰ The control experiment of a bare gold surface only shows small signals from adventitious carbon at 284.8, 286.2, and 288.6 eV, corresponding to C=C, C-O, and C=O, respectively. Thus, the C 1s XPS provides evidence of the desired structures based

on substantially increased intensities at expected peak locations. The isocyanate impurity would be indicated by a C 1s peak at 287.9 eV, ²⁰ and each Rh(I) diisocyanide film does have a small, broad peak in that area, although intensities are not much larger than the C=O peak in the control gold surface and therefore may correspond to adventitious carbon, especially considering the lack of isocyanate in the PM-IRRAS data

High-resolution N 1s XPS (Figure 4) is also useful for assessing the purity of the isocyanide structural unit because degradation to isocyanate or polyisocyanide functional groups is indicated by a diagnostic shift from 400.2 to 399.2 or 399.5 eV, respectively. The main N 1s feature is seen at 400.2 eV, with smaller peaks within the range of 399.1–399.5 eV. The presence of these lower energy peaks indicates some degree of deterioration of the Rh(I)-isocyanide-based structure; however, the isocyanide N 1s signal is still dominant. This result is in contrast with the reported XPS data for monolayers of aromatic isocyanides on gold and for Rh(I) PDI polymers obtained via powder synthesis; in these prior reports, the degradation peaks at 399.3 and 400.1 eV are the major N 1s features after limited air exposure. ^{20,25}

Air-Free Synthesis. Because PM-IRRAS and XPS data suggested the presence of polyisocyanide impurities in the films, a film was prepared by method B to exclude components of air that may cause isocyanide polymerization to polyisocyanides. The films prepared under air- and water-free conditions do not show any polyisocyanide or isocyanate signals in their PM-IRRAS data (Figure S2 and S3). PM-IRRAS of the seed BPDI layer and multilayers of Rh(I) BPDI prepared by method B show stronger Rh(I)-bound diisocyanide C≡N stretches compared to those prepared under ambient conditions (Figure 3a−c). Ellipsometry data corroborate thickness increases of more than one layer per dipping cycle (Figure S9). This result suggests that air exposure during preparation plays a major role in polyisocyanide formation with diisocyanides.

Electrochemical Studies. To evaluate the feasibility of these surface-attached coordination polymers for electrocatalysis or sensing applications, the cathodic stability of the multilayer films was tested using cyclic voltammetry in acetonitrile with a 0.1 M TBAPF₆ supporting electrolyte in the presence of decamethylferrocene (Fc*). The Rh(I) BPDI film prepared by method B was tested initially to avoid the influence of polyisocyanide impurities on the behavior (Figure 6), and subsequently, 10-layer thick films of Rh(I) PDI, Rh(I) BPDI, and Rh(I) TPDI prepared under ambient conditions were tested (Figure S7).

The voltammetry experiment starting with sweeps over narrow potential windows shows only a small response to the decamethylferrocene (Fc*) internal standard. This is attributed to the film blocking the molecules in solution from penetrating to the electrochemically active electrode material. Decamethylferrocene, with its widest cross section being 8.24 Å, 27 is small enough to penetrate the pores of the framework, which would be expected to be about the length of the diisocyanide linkers, 8.3, 14.1, and 20 Å for the PDI, BPDI, and TPDI linkers, respectively. However, diffusion within the polycrystalline framework is expected to be limited compared with a freely diffusive molecule at a flat electrode surface, and thus, a pin-hole free film would be expected to show large $\Delta E_{\rm peak}$ for the Fc*/Fc*+ couple. Over the course of the experiment, the potential is swept to successively more negative voltages until

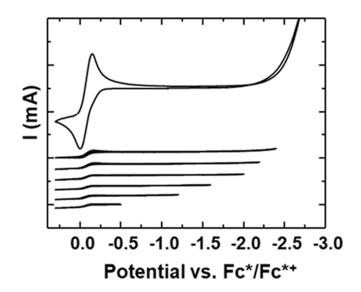


Figure 6. Cyclic voltammetry scans of the 10-layer Rh(I) BPDI film prepared in glovebox conditions by method B. Scanning to successively lower potentials reveals a breakdown voltage for the film -2.4~V~vs~Fc*.

the film is stripped at strongly cathodic potentials. Prior to successive scans reaching breakdown voltage, the decamethylferrocene internal standard signal was as much as 10-fold smaller than post-breakdown voltage and compared to a control gold sample. The breakdown potential was approximated as the cathodic potential at which the subsequent cathodic and anodic scans showed a much higher current response for the Fc*/Fc*+ redox couple; in the case of the Rh(I) BPDI film, this did not occur until a potential beyond -2.4 V versus Fc*. For these films, the breakdown potentials ranged from -1.4 to -2.4 V versus Fc*, possibly from defect formations during film formation. Impurities from air reactivity or patchiness of films may play a role, and thus, future applications with such films should entail preparation procedures to protect the materials from air. In comparison with alkanethiol SAMs, which show reductive desorption to form thiolates at modest potentials, ²⁸ the breakdown stripping potentials of the Rh diisocyanide films reported here indicate cathodically robust films, and no obvious reduction signals apart from the solvent window appear in the voltammograms. This seems to indicate a non-Faradaic process responsible for film breakdown. This could arise from some material decomposition of the deposited film, including pinhole formation, cracking, delamination, or chemical erosion. To investigate this, after the electrochemical experiments, PM-IRRAS and XPS measurements were taken of the Rh(I) BPDI film sample (Figure S5 and S8). The distinct C≡N stretches are no longer observed after electrochemical experiments, suggesting that the Rh(I) BPDI film is no longer on the Au substrate. The N 1s and Rh 3d XPS spectra show a loss of signal, further confirming that the Rh(I) BPDI film is no longer bound to the Au substrate, suggesting a complete decomposition or delamination pathway.

CONCLUSIONS

In summary, we have prepared and characterized diisocyanide linked SAM coordination polymers on Au(111) constructed by layer-by-layer epitaxial growth that are electrochemically stable to up to -2.2 V versus Fc*. The characterization of these materials is consistent with the successful growth of the films one layer at time. PM-IRRAS analysis indicates that protection from air during synthesis minimizes the formation of polyisocyanide impurities. XPS data show that a small degree of radical-initiated degradation occurs with prolonged air exposure, leading to a similar indication of polyisocyanide impurities regardless of the preparation environment. Previous reports on SAMs of diisocyanides or untethered Rh(I) diisocyanide coordination polymers prepared as powders

have implicated isocyanate groups or polyisocyanides as major degradation products, but given that there is no evidence for the presence of these impurities in our surface-immobilized films, it is hypothesized that the integration of the diisocyanides into this surface-bound multilayer framework makes them less vulnerable to reaction in air compared to powder versions with more exposed surface areas.

The stability of these films at moderately high potentials suggests that the incorporation of redox-active metals in place of the Rh(I) nodes or at other attachment sites doped with multi-functional diisocyanides could lead to further development of these protective films with interesting tailorable electrochemical properties. Further development can also be directed toward multiple applications, such as sensors or electrochemical reduction catalysis for the transformation of small molecules. Future work will be focused on incorporating electrochemically active sites in the linkers using different ligand motifs and on developing similar layer-by-layer deposition for coordination polymers based on more abundant metals.

ASSOCIATED CONTENT

Supporting Information

The Supporting Information is available free of charge at https://pubs.acs.org/doi/10.1021/acs.jpcc.2c05079.

PM-IRRAS, CV, XPS, ellipsometry, PXRD, and SEM images (PDF)

AUTHOR INFORMATION

Corresponding Author

Clifford P. Kubiak — Department of Chemistry and Biochemistry, University of California, San Diego, La Jolla, California 92093, United States; orcid.org/0000-0003-2186-488X; Phone: (858) 822-2665; Email: ckubiak@ucsd.edu

Authors

Gwendolynne L. Lee – Department of Chemistry and Biochemistry, University of California, San Diego, La Jolla, California 92093, United States

Thomas Chan — Department of Nanoengineering, University of California, San Diego, La Jolla, California 92093, United States

Joseph M. Palasz – Department of Chemistry and Biochemistry, University of California, San Diego, La Jolla, California 92093, United States

Complete contact information is available at: https://pubs.acs.org/10.1021/acs.jpcc.2c05079

Author Contributions

G.L.L. and T.C. contributed equally. The manuscript was written through contributions of all authors. All authors have given approval to the final version of the manuscript.

Notes

The authors declare no competing financial interest.

ACKNOWLEDGMENTS

XPS work was performed at the UC Irvine Materials Research Institute (IMRI) using instrumentation funded in part by the National Science Foundation Major Research Instrumentation Program under grant no. CHE-1338173. This work was performed in part at the San Diego Nanotechnology

Infrastructure (SDNI) of UCSD, a member of the National Nanotechnology Coordinated Infrastructure (NNCI), which is supported by the National Science Foundation (Grant ECCs-15421478). The authors gratefully acknowledge financial support from the NSF, under CHE-1853908.

REFERENCES

- (1) Centi, G.; Perathoner, S. Opportunities and prospects in the chemical recycling of carbon dioxide to fuels. *Catal. Today* **2009**, *148*, 191–205.
- (2) Sheehan, S. W.; Thomsen, J. M.; Hintermair, U.; Crabtree, R. H.; Brudvig, G. W.; Schmuttenmaer, C. A. A molecular catalyst for water oxidation that binds to metal oxide surfaces. *Nat. Commun.* **2015**, *6*, 6469.
- (3) Jin, T.; Liu, C.; Li, G. Heterogenization of a macrocyclic cobalt complex for photocatalytic CO2 reduction. *J. Coord. Chem.* **2016**, *69*, 1748–1758.
- (4) Sato, S.; Namba, K.; Hara, K.; Fukuoka, A.; Murakoshi, K.; Uosaki, K.; Ikeda, K. Kinetic Behavior of Catalytic Active Sites Connected with a Conducting Surface through Various Electronic Coupling. J. Phys. Chem. C 2016, 120, 2159–2165.
- (5) Dunand-Sauthier, M. C.; Deronzier, A.; Moutet, J.; Tingry, S. Electrosynthesis and co-ordination chemistry of polymer films coated on electrode surfaces from pyrrole polypyridyls. *J. Chem. Soc., Dalton Trans.* 1996, 12, 2503–2509.
- (6) O'Toole, T. R.; Sullivan, P. B.; Bruce, M. R.-M.; Margerum, L. D.; Murray, R. W.; Meyer, T. J. Electrocatalytic reduction of CO2 by a complex of rhenium in thin polymeric films. *J. Electroanal. Chem.* 1989, 259, 217–239.
- (7) Feinstein-Jaffe, I.; Efraty, A. Electrical semiconductivity of stacked layer coordination polymers of rhodium(I). *Macromolecules* **1986**, *19*, 2076–2077.
- (8) Hod, I.; Sampson, M. D.; Deria, P.; Kubiak, C. P.; Farha, O. K.; Hupp, J. T. Fe-Porphyrin-Based Metal-Organic Framework Films as High-Surface Concentration, Heterogeneous Catalysts for Electrochemical Reduction of CO2. ACS Catal. 2015, 5, 6302–6309.
- (9) Kornienko, N.; Zhao, Y.; Kley, C. S.; Zhu, C.; Kim, D.; Lin, S.; Chang, C. J.; Yaghi, O. M.; Yang, P. Metal-Organic Frameworks for Electrocatalytic Reduction of Carbon Dioxide. *J. Am. Chem. Soc.* **2015**, 137, 14129–14135.
- (10) Zhanaidarova, A.; Jones, S. C.; Despagnet-Ayoub, E.; Pimentel, B. R.; Kubiak, C. P. Re(tBu-bpy)(CO)3Cl Supported on Multi-Walled Carbon Nanotubes Selectively Reduces CO2 in Water. *J. Am. Chem. Soc.* **2019**, *141*, 17270–17277.
- (11) Zhang, X.; Wu, Z.; Zhang, X.; Li, L.; Li, Y.; Xu, H.; Li, X.; Yu, X.; Zhang, Z.; Liang, Y.; et al. Highly selective and active CO2 reduction electrocatalysts based on cobalt phthalocyanine/carbon nanotube hybrid structures. *Nat. Commun.* 2017, 8, 14675.
- (12) Wang, M.; Torbensen, K.; Salvatore, D.; Ren, S.; Joulié, D.; Dumoulin, F.; Mendoza, D.; Lassalle-Kaiser, B.; Işci, U.; Berlinguette, C. P.; et al. CO2 electrochemical catalytic reduction with a highly active cobalt phthalocyanine. *Nat. Commun.* **2019**, *10*, 3602.
- (13) Robin, A. Y.; Fromm, K. M. Coordination polymer networks with O- and N-donors: What they are, why and how they are made. *Coord. Chem. Rev.* **2006**, 250, 2127–2157.
- (14) Stock, N.; Biswas, S. Synthesis of Metal-Organic Frameworks (MOFs): Routes to Various MOF Topologies, Morphologies, and Composites. *Chem. Rev.* **2012**, *112*, 933–969.
- (15) Sun, L.; Campbell, M. G.; Dincă, M. Electrically Conductive Porous Metal-Organic Frameworks. *Angew. Chem., Int. Ed.* **2016**, *55*, 3566–3579.
- (16) Bullock, R. M.; Das, A. K.; Appel, A. M. Surface Immobilization of Molecular Electrocatalysts for Energy Conversion. *Chem.—Eur. J.* **2017**, 23, 7626–7641.
- (17) Liu, W.; Yin, X.-B. Metal-organic frameworks for electrochemical applications. *TrAC, Trends Anal. Chem.* **2016**, *75*, 86–96.

- (18) Mann, K. R.; Gordon, J. C. I.; Gray, H. B. Characterization of oligomers of tetrakis(phenyl isocyanide)rhodium(I) in acetonitrile solution. *J. Am. Chem. Soc.* 1975, 97, 3553–3555.
- (19) Chen, Y.; Li, K.; Lloyd, H. O.; Lu, W.; Chui, S. S.; Che, C. M. Tetrakis(arylisocyanide) Rhodium(I) Salts in Water: NIR Luminescent and Conductive Supramolecular Polymeric Nanowires with Hierarchical Organization. *Angew. Chem., Int. Ed.* **2010**, *49*, 9968–9971.
- (20) Carson, C. G.; Gerhardt, R. A.; Tannenbaum, R. Chemical Stability and Characterization of Rhodium-Diisocyanide Coordination Polymers. *J. Phys. Chem. B* **2007**, *111*, 14114–14120.
- (21) Goldeman, W.; Nasulewicz-Goldeman, A. Synthesis and antiproliferative activity of aromatic and aliphatic bis-[aminomethylidene(bisphosphonic)] acids. *Bioorg. Med. Chem. Lett.* **2014**, 24, 3475–3479.
- (22) Hong, S.; Reifenberger, R.; Tian, W.; Datta, S.; Henderson, J. I.; Kubiak, C. P. Molecular conductance spectroscopy of conjugated, phenyl-based molecules on Au(111): the effect of end groups on molecular conduction. *Superlattices Microstruct.* **2000**, 28, 289–303.
- (23) Henderson, J. I.; Feng, S.; Bein, T.; Kubiak, C. P. Adsorption of Diisocyanides on Gold. *Langmuir* **2000**, *16*, 6183–6187.
- (24) Dart, J. W.; Lloyd, M. K.; Mason, R.; McCleverty, J. A. Isocyanide complexes of rhodium and iridium. Part I. Tetrakisisocyanide species, their oxidative addition reactions, and some allyl complexes. *J. Chem. Soc., Dalton Trans.* 1973, 2039.
- (25) Stapleton, J. J.; Daniel, T. a.; Uppili, S.; Cabarcos, O. M.; Naciri, J.; Shashidhar, R.; Allara, D. L. Self-Assembly, Characterization, and Chemical Stability of Isocyanide-Bound Molecular Wire Monolayers on Gold and Palladium Surfaces. *Langmuir* **2005**, *21*, 11061–11070.
- (26) DuBose, D. L.; Robinson, R. E.; Holovics, T. C.; Moody, D. R.; Weintrob, E. C.; Berrie, C. L.; Barybin, M. V. Interaction of Monoand Diisocyanoazulenes with Gold Surfaces: First Examples of Self-Assembled Monolayer Films Involving Azulenic Scaffolds. *Langmuir* **2006**, 22, 4599–4606.
- (27) Sanjuan-Szklarz, W. F.; Hoser, A. A.; Gutmann, M.; Madsen, A. O.; Woźniak, K. Yes, one can obtain better quality structures from routine X-ray data collection. *IUCrJ* **2016**, 3, 61–70.
- (28) Walczak, M. M.; Popenoe, D. D.; Deinhammer, R. S.; Lamp, B. D.; Chung, C.; Porter, M. Reductive desorption of alkanethiolate monolayers at gold: a measure of surface coverage. *Langmuir* **1991**, *7*, 2687–2693.